Energy Storage Hot Paper

Deutsche Ausgabe: DOI: 10.1002/ange.201508293
Internationale Ausgabe: DOI: 10.1002/anie.201508293

A Shape-Memory Supercapacitor Fiber

*Jue Deng, Ye Zhang, Yang Zhao, Peining Chen, Xunliang Cheng, and Huisheng Peng**

Abstract: *A shape-memory, fiber-shaped supercapacitor is developed by winding aligned carbon nanotube sheets on a shape-memory polyurethane substrate. Despite its flexibility and stretchability, the deformed shapes under bending and stretching can be "frozen" as expected and recovered to the original state when required. Its electrochemical performances are well-maintained during deformation, at the deformed state and after the recovery.*

Portable and wearable electronics have been rapidly developed and may be widely used in future life.[1–6] To meet the diverse demands of these electronic devices, it is critical to fabricate high-performance, multifunctional, adaptable energy storage systems to power them.[6–13] To this end, flexible energy storage devices have attracted abundant attention and can be deformed into specific shapes that are recovered to the previous states upon the removal of external forces.[13–18] However, it is also necessary while unavailable to "freeze" the deformed shape in a variety of fields,[19–22] for example, the same fiber-shaped devices are expected to satisfy non-standard surfaces such as bodies of different people by performing deformations under an external force and further maintaining them after removing the external force.

Herein, for the first time, a new shape-memory, fiber-shaped supercapacitor (SFSC) is produced by wrapping aligned carbon nanotube (CNT) sheets onto a shape-memory polyurethane (SMP) substrate. As shown in Figure 1, the SFSC can be transformed and "frozen" into user-required shapes and sizes; it can recover to the original shape and size automatically once the temperature exceeds the thermal transition temperature (T_{tran}).[20,21] The electrochemical performances are well maintained during deformation, at the "frozen" state and after the shape recovery. The SFSCs have been further woven in electronic textiles to fabricate smart clothes for flexible electronic devices.

The fabrication process of the SFSC is schematically shown in Figure S1 in the Supporting Information. An SMP fiber was first prepared through a wet spinning method and wound with aligned CNT sheets to produce the shape-memory electrode. Here the aligned CNT sheet had been dry-drawn from an aligned CNT array synthesized by chemical vapor deposition.[23,24] The shape-memory electrode was coated with a layer of poly(vinyl alcohol) (PVA) gel electrolyte, followed by winding another layer of aligned CNTs as the outer electrode. Another thin layer of gel electrolyte was further coated to obtain the SFSC. The gel electrolyte also served as a separator, and it should be dried before winding the second layer of CNT sheets to prevent short circuits.

Figure 2a shows a typical scanning electron microscopy (SEM) image of the shape-memory fiber that served as the inner electrode. The aligned CNTs can be stably attached on the polyurethane fiber and the smooth surface of the fiber substrate was favorable to uniformly wrapping aligned CNTs and maintaining the orientation (Figure 2b and S2). Figure 2c and 2d verify that the gel electrolyte could serve as an effective separator as the two layers of aligned CNT sheets were efficiently infiltrated with and separated by the gel electrolyte. This coaxial architecture provides a high stability in both structure and property for the SFSC during and after deformation.

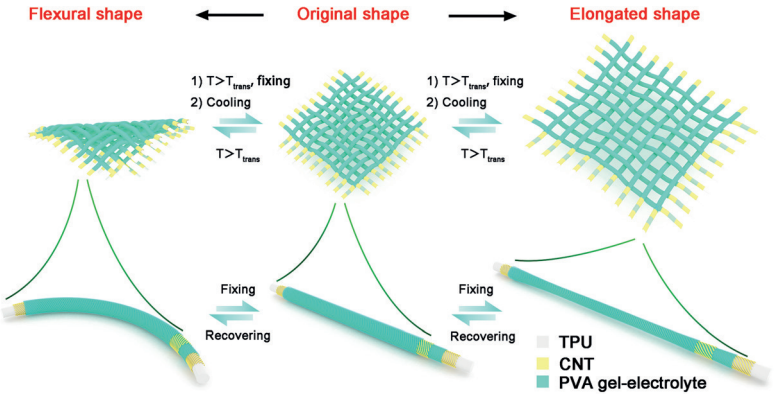

Figure 1. Schematic of the SFSC and the resulting textile that are reversibly transformed into flexural or elongated states and recovered to the original shape.

The stability of the shape-memory electrode during deformation played a critical role for the SFSC. Three different helical angles of 45, 60, and 75° were compared with the other parameters remaining unchanged, that is, a diameter of 900 μm for the shape-memory fiber and a thickness of 560 nm for the aligned CNT layer. After being deformed and fixed with different radii of curvatures, no detectable resistance changes were observed for the three

[*] J. Deng,[+] Y. Zhang,[+] Y. Zhao, P. Chen, Dr. X. Cheng, Prof. Dr. H. Peng
State Key Laboratory of Molecular Engineering of Polymers
Department of Macromolecular Science and
Laboratory of Advanced Materials, Fudan University
Shanghai 200438 (China)
E-mail: penghs@fudan.edu.cn
Prof. Dr. H. Peng
State Key Laboratory for Modification of Chemical Fibers
and Polymer Materials, Donghua University Shanghai
201620 (China)
[+] These authors contributed equally to this work.

Supporting information for this article is available on the WWW under http://dx.doi.org/10.1002/anie.201508293.

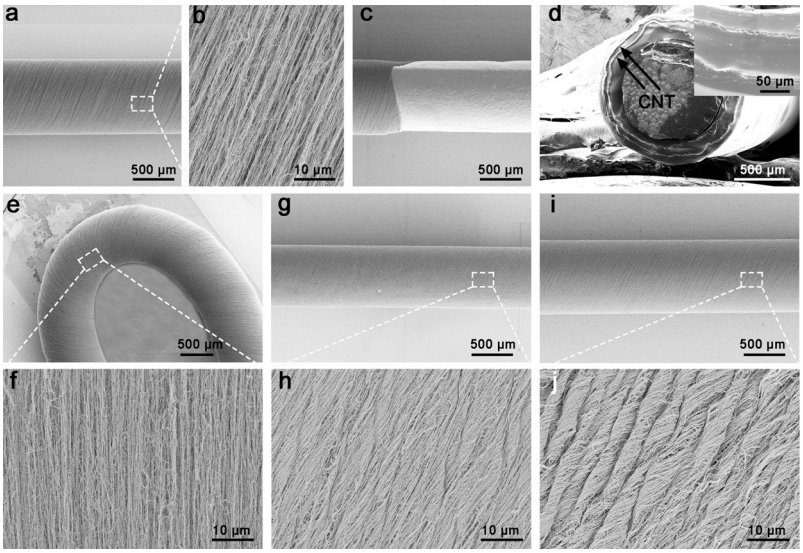

Figure 2. Scanning electron microscopy (SEM) images of the SFSC. a,b) Shape-memory electrode at low and high magnifications, respectively. c) The surface of the PVA gel electrolyte and the border between the PVA gel electrolyte and aligned CNTs. d) Cross-sectional image of the SFSC (inset, high magnification). e,f) A flexural shape of SFSC electrode at low and high magnifications, respectively. g,h) An SFSC electrode being stretched by 50%. i,j) A recovered shape of the SFSC electrode at (g).

helical angles (Figure S3). The stable structure at flexural and recovered states was also verified by Figure 2 e and 2 f. Owing to the physical crosslink in the switching phases, the shape-memory electrode was able to deform and maintain the elongated states at strains of 25, 50, 75, and 100%. The electrical resistances of the shape-memory electrodes were slightly increased by about 0.5 kΩ during stretching with a strain of 100% at both 60° and 75°, and they were also returned after the shape recovery. However, the electrical resistances were dramatically and irreversibly increased by about 2000% at a low helical angle of 45° (Figure S4). Considering the relatively lower resistance at 60° than 75°, a wrapping helical angle of 60° was used below unless otherwise specified. The SEM images also verified the stable structure of the shape-memory electrode at elongated and recovered states (Figure 2 g–j).

The SFSC was then fabricated from the shape-memory electrode and PVA gel electrolyte. To obtain high-performance SFSCs, the thickness of the CNT electrode was first investigated. The specific capacitances calculated from the galvanostatic charging and discharging curves were increased from 11 to 24 $F g^{-1}$ with the increasing thickness of CNT layer from 140 to 560 nm and then decreased to 17 $F g^{-1}$ with further increase in thickness because of the inadequate contact between the inner CNT and gel electrolyte (Figures S5 and S6). Therefore, the shape-memory electrode with the CNT thickness of 560 nm was used for the SFSC. The length and volumetric specific capacitances were 0.269 $mF cm^{-1}$ and 42.3 $mF cm^{-3}$, respectively. They were comparable with the other supercapacitors based on carbon materials.[8,13,14] Cyclic voltammetry (CV) measurement was then performed to characterize the electrochemical property, and the CV curves shared a rectangular shape that indicated a double-layer capacitor. With the increasing scan rates of 50, 100, and 300 to 500 $mV s^{-1}$, the rectangular shapes were well maintained, indicating a low internal resistance and high performance during the rapid charging and discharging process (Figure S7). The galvanostatic charge–discharge curves retained a symmetrical triangle shape at increasing current densities from 0.1 to 1.0 $A g^{-1}$, indicating a high stability (Figure S8). Moreover, the coulombic efficiencies of the supercapacitor were maintained by over 90% at the current density from 0.1 to 1 $A g^{-1}$, indicating a high reversibility. To understand the electrochemical stability of the SFSC, the cyclic charging and discharging characterization was carried out at a current density of 1 $A g^{-1}$, and no obvious attenuations in capacitance had been observed after 12000 cycles (Figure S9).

The SFSC can be programmed into a variety of shapes to adapt to different working conditions. As shows in Figure 3 a, the SFSC was deformed and shaped with increasing radii of curvatures under external bending stresses when the temperature exceeded T_{trans}. After cooled down to room temperature, the polymer network of polyurethane was physically cross-linked and "frozen" to maintain the flexural shape. Upon heating at a temperature equal to or beyond T_{trans}, the physical crosslinks in the middle phase were cleaved, and the full recovery of the SFSC was achieved. The T_{trans} values can be tuned to satisfy various applications by choosing different shape-memory materials such as the other polymers or alloys.

The electrochemical performances of the SFSC under different flexural deformations were carefully investigated. After being shaped into flexural shapes with increasing radii of curvatures ranging from 1.5 to 4 cm, the SFSC was able to work properly; the overlapped galvanostatic charging and discharging curves also verified that the specific capacitances remained unchanged in flexural shapes (Figure 3 b). After being heated to T_{trans} or higher, the flexural SFSC was recovered to the original linear shape, and almost the same CV curves indicated a high stability before and after shape recovery (Figure 3 c). Furthermore, the dependence of the specific capacitance on deformation and recovery cycle number was traced, and no detectable decrease in specific capacitance had been found after repeating shape deformation and recovery for twenty cycles (Figure 3 d). Even under a dynamically shape-recovering process, the SFSC can work effectively (Figure 3 e). The smooth galvanostatic charging and discharging curve demonstrated that the electrochemical performance of the SFSC was stable.

Besides deforming into different flexural shapes, the SFSC can be programmed into elongated states. The strain recovery rate plays an important role in studying the ability of the SFSC to memorize its original shape.[21] Here the strain recovery rate (R_r) was calculated accordingly to the equation of $R_r = \Delta L/\Delta L_0 \times 100\%$. Here ΔL was the length change when the shape-memory effect occurred, while ΔL_0 was the length change when the SFSC was programmed into an

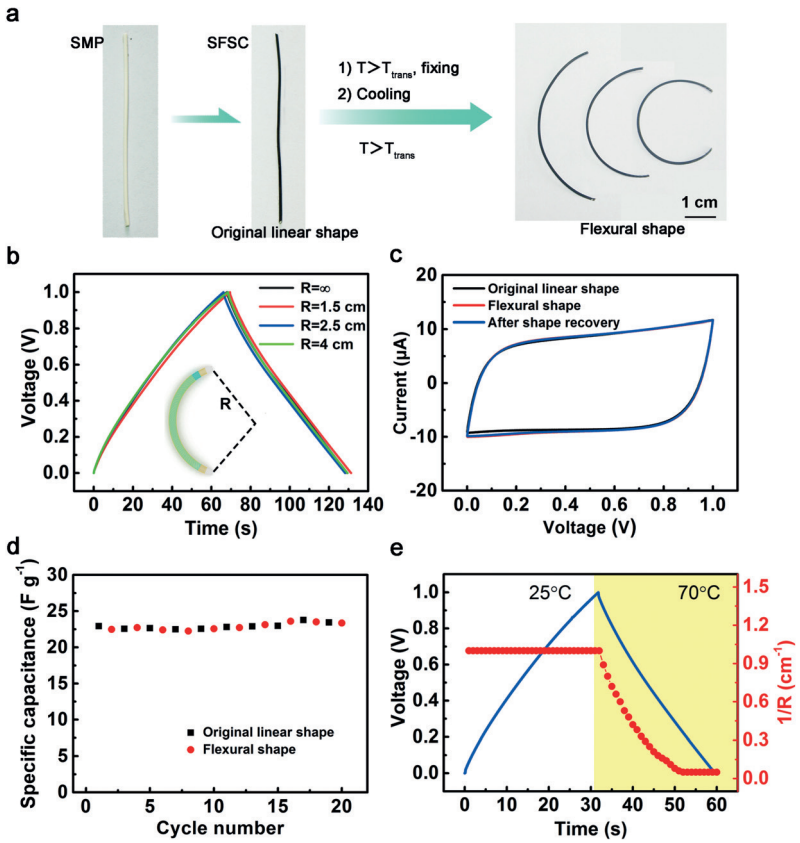

Figure 3. SFSC under flexural deformation and shape recovery. a) A photograph and b) galvanostatic charging and discharging curves of the SFSC at different flexural shapes. The galvanostatic charging and discharging tests were performed at a current density of 0.1 A g^{-1}. c) Cyclic voltammetry (CV) curves of the SFSC before and after flexural deformation and shape recovery. The CV tests were carried out at a scan rate of 0.5 V s^{-1}. d) Dependence of the specific capacitance on deformation cycle number. The specific capacitance was calculated from the charging and discharging curve at the current density of 0.2 A g^{-1}. e) Galvanostatic charging and discharging curves of the SFSC under a dynamic shape-recovering process at a current density of 0.2 A g^{-1}.

elongated state. Figure 4a shows that the elongated states with strains of 25, 50, 75, and 100% have been well maintained, and the strain recovery rate exceeded 90% for each case. As shown in Figure 4b, the capacitance of the SFSC was also well maintained. SEM images under stretching had further verified its stability (Figure S10). Even at the strain of 100%, the capacitance can be maintained by above 80%. Beyond the transformation temperature, the SFSC can fully recover to the original length, and the galvanostatic charging and discharging curves were overlapped before and after elongation and shape recovery (Figure 4c). The performance of the SFSC was traced for 500 cycles of deformation and recovery at a strain of 50%, and no obvious decreases in electrochemical property had been detected (Figure 4d).

The SFSC can be also deformed into various complex architectures by combining the bending and elongating process, for example, hexagram and helix (Figure 5a). Besides, the fiber shape provided the SFSC with several promising advantages, for example, it can be further woven into electronic textiles. The electrochemical performances of SFSC textiles that were connected in series and parallel were also investigated. As shown in Figure 5b and 5c, when three SFSCs were assembled in series or parallel, the galvanostatic voltage or discharging time was about three times of the individual SFSC, respectively. Of course, the resulting textile from the SFSCs had also a shape memory and could be "frozen" into different user-required shapes and sizes (Figure 5d).

In summary, a shape-memory, fiber-shaped supercapacitor is developed by winding aligned CNT sheets on a shape-memory polyurethane substrate. Despite its flexiblity and stretchability, the deformed shapes under bending and stretching can be maintained as expected and further recovered to the original state when required. The electrochemical performances of the fiber-shaped supercapacitors have been well maintained during deformation, at the deformed state and after the recovery. These energy storage fibers are further woven into smart electronic textiles that are particularly attractive to the next-generation wearable electronics. This strategy can be extended to the other fiber-shaped energy harvesting and storage devices and electronic devices; it can be also used to fabricate a variety of planar shape-memory energy and electronic devices.

Experimental Section

Preparation of shape-memory fiber: Thermoplastic polyurethane (TPU, Huntsman A70e4675) was dissolved in dimethyl formamide (DMF) with a concentration of 0.6 g mL^{-1} at 80°C for 1 h under mechanical stirring. After cooled down to room temperature, the resulting viscous solution was injected into a DMF/water coagulation bath (v/v, 6/4) at a speed of 3.5 mm min^{-1} through a 20 mL single-hole spinneret.[25] The resulting polyurethane fiber was immersed in the coagulation bath for 10 minutes and then transferred to distilled water for further coagulation. The shape-memory fiber was finally prepared after drying at 60°C for 1 h.

Fabrication of shape-memory supercapacitor fiber: Spinnable CNT arrays were first synthesized by chemical vapor deposition.[23,24] Two ends of the polyurethane fiber were then fixed on two motors, and a CNT array was stabilized on a motorized translation stage. Continuous aligned CNT sheet (thickness of ca. 18 nm) was drawn from the CNT array and attached on the fixed shape-memory polyurethane fiber with angles of 45, 60, and 75°. The two motors and the translation stage were operated simultaneously. The winding velocity of aligned CNT sheet was maintained to be equal to the moving velocity of translation stage, so the helical angle of the aligned CNT sheet was maintained across the fiber during wrapping. PVA (1 g) was dissolved in distilled water (9 g) at 90°C for 2 h, followed by addition of H_3PO_4 aqueous solution (85 wt%, 1 g) and cooling down to room temperature.[26] The PVA gel electrolyte was uniformly coated onto the fiber, followed by vacuum heating at 80°C for 10 minutes. The above coating process was repeated for three times. The CNT sheet was wound again onto the electrolyte as the other electrode, followed by coating another layer of electrolyte to obtain the SFSC. The specific capacitance (C) for SFSC was calculated from the equation of $C = 4 \times I \times t/(M \times U)$, where I, t, M, and U correspond to the discharge current, discharge time, the mass of one CNT electrode, and the potential window, respectively.

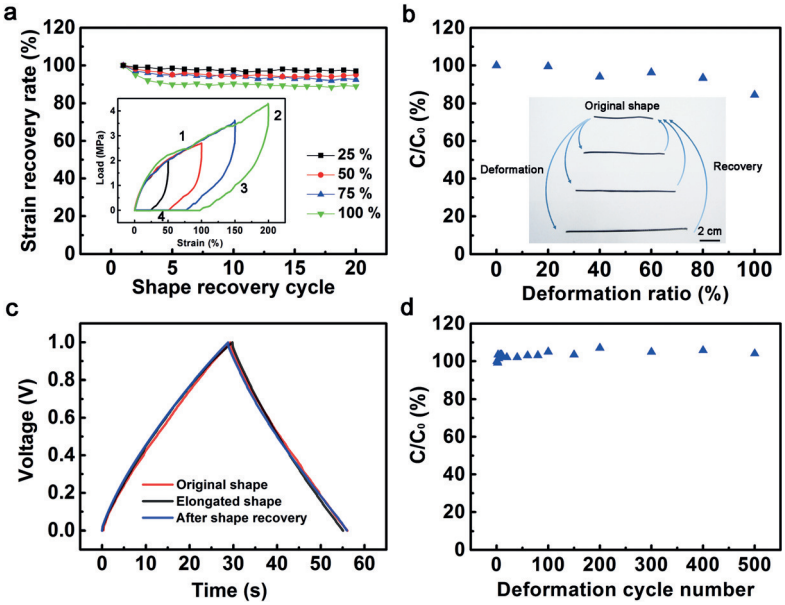

Figure 4. SFSC under elongated deformation and shape recovery. a) Dependence of shape recovery ratio on shape recovery cycle number. The inserted stress-strain curves compared the shape-memory effect (part 1, stretching to the maximum strain at T_{trans}; part 2, cooling down to room temperature when the maximum strain was maintained; part 3, releasing the stress; part 4, heating up to T_{trans}). b) Dependence of capacitance ratio on deformation ratio. c) Galvanostatic charging and discharging curves of the SFSC before and after elongated deformation with a strain of 50% and shape recovery. The galvanostatic charging and discharging tests were performed at a current density of 0.2 $A g^{-1}$. d) Dependence of the capacitance ratio on the deformation cycle number. C_0 and C correspond to specific capacitances before and after stretching at both (b) and (d), respectively.

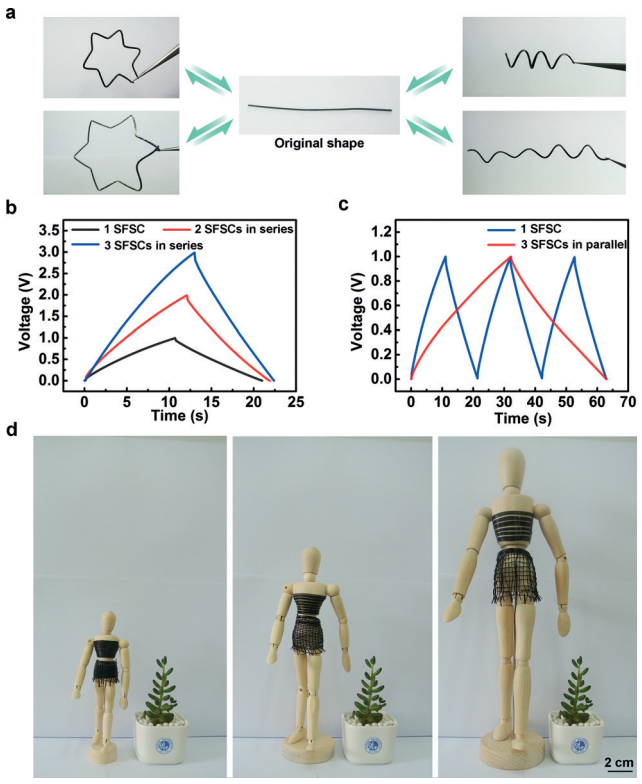

Figure 5. a) Photographs of an SFSC transformed into different shapes and sizes. b,c) Galvanostatic charging and discharging curves of SFSCs arranged in series and parallel, respectively. The galvanostatic charging and discharging tests were performed at a current density of 0.5 $A g^{-1}$. d) Photographs of the same smart clothes woven from SFSCs that were "frozen" into different shapes and sizes.

Acknowledgements

This work was supported by MOST (grant number 2011CB932503), NSFC (grant number 21225417), STCSM (grant number 15XD1500400), the Fok Ying Tong Education Foundation, the Program for Outstanding Young Scholars from the Organization Department of the CPC Central Committee, and the visiting fund from State Key Laboratory for Modification of Chemical Fibers and Polymer Materials.

Keywords: carbon nanotubes · energy storage · polymers · shape memory · supercapacitors

How to cite: *Angew. Chem. Int. Ed.* **2015**, *54*, 15419–15423
Angew. Chem. **2015**, *127*, 15639–15643

[1] S. Bauer, S. Bauer-Gogonea, I. Graz, M. Kaltenbrunner, C. Keplinger, R. Schwödiauer, *Adv. Mater.* **2014**, *26*, 149–162.
[2] T. Chen, L. Qiu, Z. Yang, H. Peng, *Chem. Soc. Rev.* **2013**, *42*, 5031–5041.
[3] Y. Meng, Y. Zhao, C. Hu, H. Cheng, Y. Hu, Z. Zhang, G. Shi, L. Qu, *Adv. Mater.* **2013**, *25*, 2326–2331.
[4] C. Hu, L. Song, Z. Zhang, N. Chen, Z. Feng, L. Qu, *Energy Environ. Sci.* **2015**, *8*, 31–54.
[5] G. Sun, J. Liu, L. Zheng, W. Huang, H. Zhang, *Angew. Chem. Int. Ed.* **2013**, *52*, 13351–13355; *Angew. Chem.* **2013**, *125*, 13593–13597.
[6] L. Kou, T. Huang, B. Zheng, Y. Han, X. Zhao, K. Gopalsamy, H. Sun, C. Gao, *Nat. Commun.* **2014**, *5*, 3754.
[7] D. Yu, K. Goh, H. Wang, L. Wei, W. Jiang, Q. Zhang, L. Dai, Y. Chen, *Nat. Nanotechnol.* **2014**, *9*, 555–562.
[8] X. Xiao, X. Peng, H. Jin, T. Li, C. Zhang, B. Gao, B. Hu, K. Huo, J. Zhou, *Adv. Mater.* **2013**, *25*, 5091–5097.
[9] J. Ren, Y. Zhang, W. Bai, X. Chen, Z. Zhang, X. Fang, W. Weng, Y. Wang, H. Peng, *Angew. Chem. Int. Ed.* **2014**, *53*, 7864–7869; *Angew. Chem.* **2014**, *126*, 7998–8003.
[10] G. Sun, X. Zhang, R. Lin, J. Yang, H. Zhang, P. Chen, *Angew. Chem. Int. Ed.* **2015**, *54*, 4651–4656; *Angew. Chem.* **2015**, *127*, 4734–4739.

[11] C. Zhu, P. Yang, D. Chao, X. Wang, X. Zhang, S. Chen, B. K. Tay, H. Huang, H. Zhang, W. Mai, *Adv. Mater.* **2015**, *27*, 4566 – 4571.
[12] X. Xiao, T. Li, P. Yang, Y. Gao, H. Jin, W. Ni, W. Zhan, X. Zhang, Y. Cao, J. Zhong, *ACS Nano* **2012**, *6*, 9200 – 9206.
[13] X. Cao, Z. Yin, H. Zhang, *Energy Environ. Sci.* **2014**, *7*, 1850 – 1865.
[14] T. Chen, R. Hao, H. Peng, L. Dai, *Angew. Chem. Int. Ed.* **2015**, *54*, 618 – 622; *Angew. Chem.* **2015**, *127*, 628 – 632.
[15] Y. Zhang, W. Bai, X. Cheng, J. Ren, W. Weng, P. Chen, X. Fang, Z. Zhang, H. Peng, *Angew. Chem. Int. Ed.* **2014**, *53*, 14564 – 14568; *Angew. Chem.* **2014**, *126*, 14792 – 14796.
[16] M. Zu, Q. Li, G. Wang, J. H. Byun, T. W. Chou, *Adv. Funct. Mater.* **2013**, *23*, 789 – 793.
[17] P. Xu, T. Gu, Z. Cao, B. Wei, J. Yu, F. Li, J. H. Byun, W. Lu, Q. Li, T. W. Chou, *Adv. Energy Mater.* **2014**, *4*, 1300759.
[18] Z. Xu, Z. Liu, H. Sun, C. Gao, *Adv. Mater.* **2013**, *25*, 3249 – 3253.
[19] E. H. Kil, K. H. Choi, H. J. Ha, S. Xu, J. A. Rogers, M. R. Kim, Y. G. Lee, K. M. Kim, K. Y. Cho, S. Y. Lee, *Adv. Mater.* **2013**, *25*, 1395 – 1400.
[20] M. Behl, M. Y. Razzaq, A. Lendlein, *Adv. Mater.* **2010**, *22*, 3388 – 3410.
[21] A. Lendlein, S. Kelch, *Angew. Chem. Int. Ed.* **2002**, *41*, 2034 – 2057; *Angew. Chem.* **2002**, *114*, 2138 – 2162.
[22] P. Miaudet, A. Derre, M. Maugey, C. Zakri, P. M. Piccione, R. Inoubli, P. Poulin, *Science* **2007**, *318*, 1294 – 1296.
[23] H. Peng, X. Sun, F. Cai, X. Chen, Y. Zhu, G. Liao, D. Chen, Q. Li, Y. Lu, Y. Zhu, *Nat. Nanotechnol.* **2009**, *4*, 738 – 741.
[24] L. Qiu, X. Sun, W. Guo, H. Peng, *Acta. Chim. Sinica* **2012**, *70*, 1523 – 1532.
[25] G. Reddy, B. Deopura, M. Joshi, *J. Appl. Polym. Sci.* **2010**, *118*, 2291 – 2303.
[26] C. Zhao, C. Wang, Z. Yue, K. Shu, G. G. Wallace, *ACS Appl. Mater. Interfaces* **2013**, *5*, 9008 – 9014.

Received: September 4, 2015
Published online: November 3, 2015

